

Geochemistry, Geophysics, Geosystems

RESEARCH ARTICLE

10.1029/2017GC007349

Key Points:

- Garlock fault slip is driven by a combination of conjugate shear, intracontinental transform, and oroclinal bending
- Specific contributions to Garlock fault slip from different drivers are determined using geologic slip rates
- Garlock fault is a mechanical bridge that stabilizes the primary plate boundary configuration

Supporting Information:

- Supporting Information S1

Correspondence to:

A. E. Hatem,
ahatem@usc.edu

Citation:

Hatem, A. E., & Dolan, J. F. (2018). A model for the initiation, evolution, and controls on seismic behavior of the Garlock fault, California. *Geochemistry, Geophysics, Geosystems*, 19, 2166–2178. <https://doi.org/10.1029/2017GC007349>

Received 20 NOV 2017

Accepted 16 JUN 2018

Accepted article online 27 JUN 2018

Published online 22 JUL 2018

A Model for the Initiation, Evolution, and Controls on Seismic Behavior of the Garlock Fault, California

Alexandra E. Hatem¹  and James F. Dolan¹ 

¹Department of Earth Sciences, University of Southern California, Los Angeles, CA, USA

Abstract We develop a model for the evolution and activity of the Garlock fault that combines elements of three previously proposed mechanisms: (1) conjugate slip to the San Andreas fault, (2) extension in the Basin and Range, and (3) bending from oblique shear in the eastern California shear zone (ECSZ). Conjugate slip is greatest in the west and decreases eastward. Conversely, extension-induced slip increases westward from the eastern termination of the fault, reaching a maximum at and to the west of the intersection with the Sierra Nevada frontal fault. Oroclinal bending provides only a small contribution to Garlock slip that increases eastward from the east-central segment. These spatiotemporally complex loading patterns may explain alternating periods of fault activity along the Garlock and neighboring faults. Moreover, these complex kinematic relationships demonstrate that the Garlock fault acts as an efficient mechanical bridge linking slip on the northern ECSZ and San Andreas fault that may have delayed or even obviated the long-hypothesized development of a new Pacific-North America plate boundary along the ECSZ-Walker Lane.

1. Introduction

Several different models have been proposed to explain the role of the sinistral, northeast- to east-striking Garlock fault in accommodating relative plate motion within the primarily dextral, NNW- to SSE-striking Pacific-North America (Pac-NAM) plate boundary in southern California. None of these models by themselves, however, provide a unified mechanical explanation for the evolution and continued activity of this major fault (Hatem & Dolan, 2015). Such understanding is critical to untangling the mechanics of fault system behavior in the kinematically complex Pac-NAM plate boundary, as well as similar plate boundaries around the world.

In this paper, we consider the geometry of the Garlock fault, together with geologic slip rates and fault initiation timing constraints, to assess the relative contributions of three different driving mechanisms suggested in previous conceptual models. We use these results to devise a unified model that encompasses elements of all three models and quantifies the contributions from each along strike. We discuss these results in light of Garlock fault evolution, the complex fault interactions that drive Garlock slip, and controls on earthquake occurrence in southern California.

2. The Garlock Fault

The sinistral Garlock fault extends for ~255 km in a broad NE to EW arc that spans more than half the width of California (Figure 1). Along its length, the Garlock exhibits notable changes in strike that have been used to separate the fault into three segments. The 100-km-long western segment, which extends from the western intersection of the Garlock fault with the San Andreas fault (SAF) to the Koehn Lake transtensional stepover, strikes ~060°. The 070°–080°-striking central segment spans the ~90-km-long distance between Koehn Lake and the eastern end of Pilot Knob Valley, near the southern end of Panamint Valley. The 65-km-long, 090°–095°-striking, eastern segment extends from the eastern end of Pilot Knob Valley to the eastern end of the Garlock fault at the southern end of the Death Valley fault system. Offsets of bedrock and structural features show that the Garlock fault has accommodated a cumulative displacement of 48–64 km (Davis & Burchfiel, 1973; Jahns et al., 1971; Monastero et al., 1997; Smith, 1962; Smith & Ketner, 1970). Surface displacement likely began in late Miocene time (Eaton, 1932), sometime after 17 Ma (Monastero et al., 1997), and likely circa 11 Ma (Andrew et al., 2014; Burbank & Whistler, 1987; Frankel et al., 2008).

Although the Garlock fault has not generated any significant earthquakes during the historic period, there is abundant evidence for recent activity (Burke & Clark, 1978; Clark, 1973; Dawson et al., 2003; Dolan et al., 2016; Ganey et al., 2012; Madugo et al., 2012; McGill et al., 2009; McGill & Sieh, 1991, 1993; Rittase et al., 2014; Roquemore et al., 1982). Specifically, geologic slip rates averaged over early Holocene-late Pleistocene

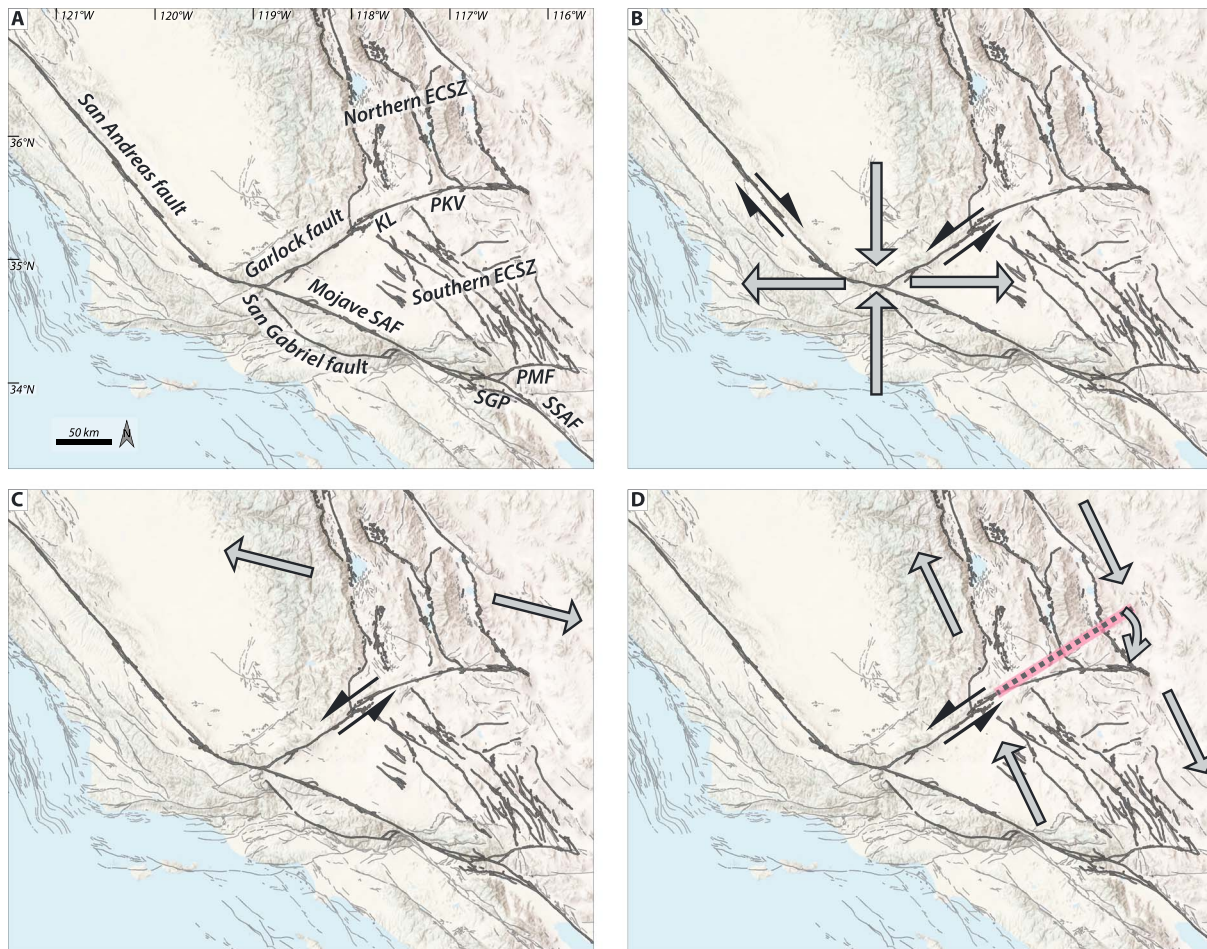


Figure 1. (a) Location map showing major faults in black; other Quaternary faults shown in pale gray (Jennings, 1994); SAF = San Andreas fault; SGK = San Gorgonio Knot; SSAF = Southern SAF; KL = Koehn Lake; PKV = Pilot Knob Valley; PMF = Pinto Mountain fault. ECSZ is eastern California shear zone. (b) Conjugate shear model in which slip on the Garlock fault is driven by interactions with the San Andreas fault. Large gray arrows show relative motion directions of key regions. (c) Extension model driven by Basin and Range extension north of the Garlock fault. (d) Oroclinal bending model driven by ECSZ dextral shear across the Garlock fault. Dashed pink line shows inferred original orientation of Garlock fault at initiation, and arrows show inferred clockwise rotation associated with NNW trending dextral ECSZ shear.

time (7–100 ka) show that the western and central segments of the fault are among the fastest-slipping faults in Southern California. These rates reveal a consistent eastward decrease in Garlock fault rate, from 7.6 ± 3.1 – 2.3 mm/year on the western segment (McGill et al., 2009), to ~ 5 – 6 mm/year on the central segment (Clark & Lajoie, 1974; Crane, 2014; Dolan et al., 2015; Ganey et al., 2012; McGill & Sieh, 1993), to $1 \pm \frac{1.5}{0.5}$ mm/year on the eastern segment (Crane, 2014). Paleoseismologic studies demonstrate that the Garlock fault has generated large-magnitude, late Holocene surface-rupturing earthquakes (Dawson et al., 2003; Madugo et al., 2012; McGill, 1992; McGill & Rockwell, 1998). Collectively, these data suggest that the Garlock experiences supercycles of strain release, characterized by variability in both earthquake occurrence and slip rates (Dawson et al., 2003; Dolan et al., 2007, 2016; Ganey et al., 2012; Rittase et al., 2014), that are potentially correlated with the behavior of other regional faults (Dawson et al., 2003; Dolan et al., 2007, 2016; Ganey et al., 2012; McAuliffe et al., 2013; Oskin et al., 2008; Peltzer et al., 2001), underscoring the importance of considering regional tectonics when devising a comprehensive model for the origin and continued activity of the Garlock fault.

3. Models of Garlock Fault Behavior

Three kinematic models have been proposed to explain the origin and evolution of the Garlock fault: (1) conjugate slip with the SAF (Hill & Dibblee, 1953), (2) intracontinental transform faulting from Basin and Range (BR) extension (Davis & Burchfiel, 1973; Troxel et al., 1972), and (3) oroclinal bending from eastern California shear zone (ECSZ) dextral shear (Garfunkel, 1974; Guest et al., 2003; Figure 2). Although each of

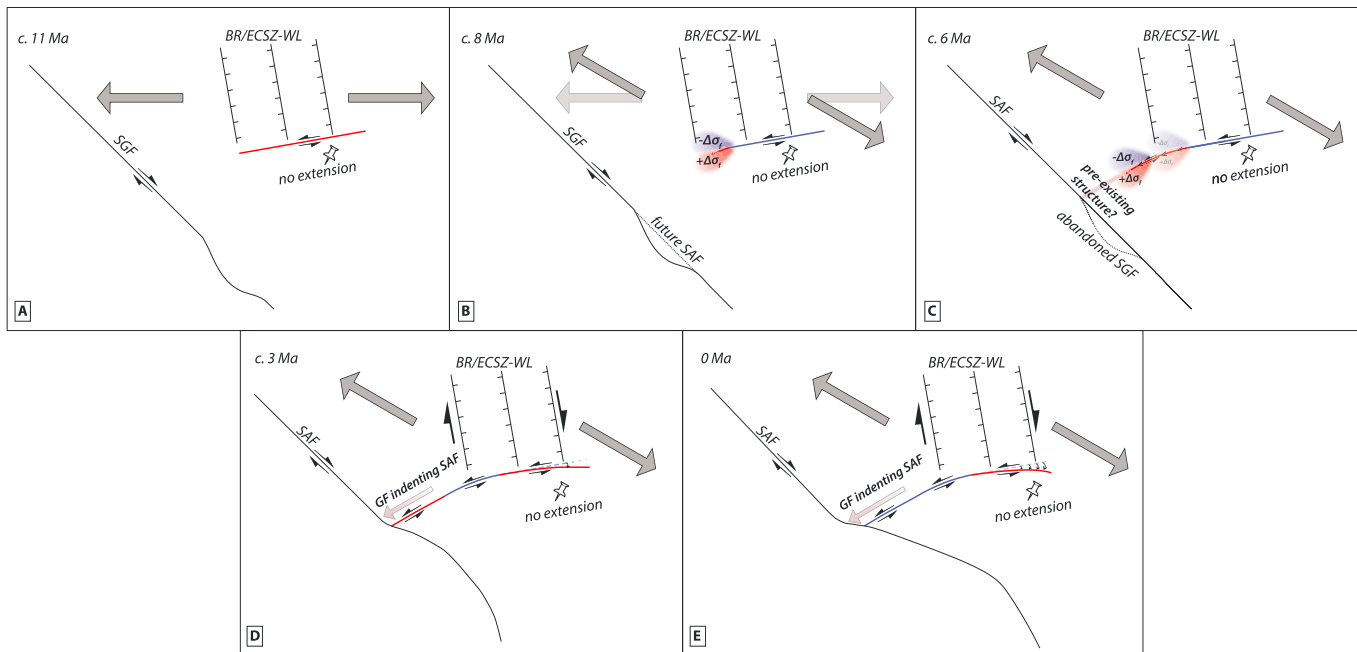


Figure 2. Proposed incremental evolution of the Garlock fault from circa 11 Ma (a), circa 8 Ma (b), circa 6 Ma (c), circa 3 Ma (d), circa 0 Ma (e), showing our preferred 075° initial strike for the central and eastern Garlock. Red lines indicate changes in Garlock fault length or geometry from previous time step; blue lines denote portions of Garlock fault unchanged from previous panel. Dark gray arrows show extension direction within the current time step; lighter gray arrows show extension direction in the previous time step, in order to highlight this change. Red lobes show positive changes in $\Delta\sigma_f$ (Coulomb stress on optimally oriented faults) that result from stresses at the tip of a propagating fault and indicate area where failure is promoted; blue lobes show negative changes in $\Delta\sigma_f$, which do not promote fault propagation.

these models highlights important aspects of the origin and current behavior of the Garlock fault, none of them alone provides a complete mechanical explanation of the Garlock fault. Garfunkel (1974), for example, postulated that there may be more than one mechanism driving the Garlock. Here we quantify these previously proposed mechanisms into a unified model for the origin and behavior of the Garlock fault.

In the first model, the Garlock fault serves as a conjugate to the San Andreas fault to accommodate the north-south shortening and east-west extrusion resulting from the mechanically inefficient 295° strike of the SAF southeast of the Big Bend, relative to the ~325° strike (DeMets et al., 2010) of Pac-NAM relative plate motion (Hill & Dibblee, 1953; King et al., 2004; Stuart, 1991) However, only the western Garlock is at a mechanically efficient conjugate (R') shear orientation with respect to the San Andreas today (McGill et al., 2009).

The second model posits that the Garlock fault behaves as an intracontinental transform fault that accommodates east-west extension of the BR north of the Garlock, relative to the nonextending Mojave block to the south (Davis & Burchfiel, 1973). Although BR extension-induced sinistral shear on the Garlock effectively explains some of the slip on the central and eastern segments of the Garlock, this model alone cannot explain the fast slip rates of the western and central Garlock fault (McGill et al., 2009).

The third model invokes clockwise oroclinal rotation of the Garlock fault in response to NNE-SSW, dextral shear in the ~80-km-wide ECSZ (Dokka & Travis, 1990a; Garfunkel, 1974; Guest et al., 2003; Humphreys & Weldon, 1994; Luyendyk, 1991; Luyendyk et al., 1980; Schermer et al., 1996). These models postulate that the entire Garlock fault initiated at the 060° present-day strike of the western Garlock, and that the central and eastern segments have rotated clockwise to their current orientations (Andrew & Walker, 2017; Andrew et al., 2014; Guest et al., 2003; McGill et al., 2009). A key limitation of this model, as discussed below, is that it applies primarily to the eastern Garlock, and minimally to the central Garlock, without contributing any slip to the fast-slipping western Garlock, which lies to the west of any ECSZ dextral shear (McGill et al., 2009).

4. A Model for Garlock Fault Evolution

We propose a comprehensive model for the evolution and ongoing activity of the Garlock fault that encompasses elements of all three earlier models and that is constrained by the current geometry and recent slip

rates of the Garlock, as well as by regional structural and geochronologic data. Sinistral Garlock fault slip likely began circa 11 Ma (Andrew et al., 2014; Figure 2a). We assume that sinistral slip initiated on the eastern and central Garlock first, primarily to accommodate intracontinental extension within the BR and ECSZ north of the Garlock, as proposed by Troxel et al. (1972) and Davis and Burchfiel (1973).

The original strike of the currently active, sinistral Garlock fault is not well constrained. If the intracontinental transform fault model is correct, then the original strike of the Garlock would be expected to be approximately parallel to the BR extension direction north of the fault (e.g., Atwater, 1970; Menard & Atwater, 1968, 1969). Regional palinspastic reconstructions indicate that, prior to initiation of the Garlock fault circa 11 Ma, extension in the region of the future Garlock fault circa 14–16 Ma was oriented approximately $\sim 075^\circ$ (McQuarrie & Wernicke, 2005; their Figure 10e); this SW-NE extension direction may have generated a WNW-trending regional fabric along which nascent faults could develop. In contrast, at 10–12 Ma, at the time of Garlock fault initiation, the BR extension direction north of the fault was approximately E-W, rotating to $\sim N75^\circ W$ by 8–10 Ma (McQuarrie & Wernicke, 2005; Snow & Wernicke, 2000; Wernicke & Snow, 1998). Following a different line of reasoning, some authors have suggested that the original orientation of the Garlock was 060° , parallel to the current orientation of the western segment of the Garlock (e.g., Guest et al., 2003; McGill et al., 2009). Thus, various proposals for the initial orientation of the Garlock fault have ranged from 090° to 060° .

An original strike of 090° for the central and eastern Garlock fault is problematic for a number of reasons. For example, this orientation would require that the currently $\sim 080^\circ$ -striking central segment would have rotated counterclockwise within the $\sim N-S$, nearly Garlock-perpendicular dextral ECSZ strain field, which seems kinematically unlikely. Moreover, an original 090° orientation would suggest that the current 090° -striking eastern segment has not rotated at all, despite being subjected to at least 3 My of dextral ECSZ shear, as well as evidence for significant clockwise rotations south of the eastern Garlock fault in the eastern Mojave region (Guest et al., 2003; Schermer et al., 1996). Finally, an original 090° orientation for the central and eastern Garlock would leave no room for subsequent northward motion of the southern Sierra Nevada, which is required by palinspastic reconstructions; these reconstructions suggest a more ENE original strike of the central and eastern Garlock ($\sim 060^\circ$ – 075° , McQuarrie & Wernicke, 2005). We therefore suggest that an original 090° strike for the central and eastern segments of the Garlock fault can be ruled out. In the following, we therefore only consider possible original orientations for the central and eastern Garlock fault of 060° and 075° , either of which is consistent with currently available constraints.

One of the most striking features of the Garlock fault is its arcuate trace (Figure 1). We suggest that as BR extension north of the Garlock continued after 11 Ma, the central Garlock fault grew southwestward along a preexisting zone of weakness, possibly along a preexisting normal fault that aided in Late Cretaceous gravitational collapse of the Sierra Nevada batholith (Blythe & Longinotti, 2013; Chapman et al., 2012; Malin et al., 1995; Wood & Saleeby, 1997; Figure 2c). This southwestward propagation was likely enhanced by the orientation of the stress field generated at the western end of the nascent fault (Figure 2b). Specifically, Coulomb failure function modeling indicates that a propagating fault will curve into the extensional stress lobe of the fault tip (e.g., Armijo et al., 2004; Bowman et al., 2003; Flerit et al., 2004; Figure 2b). Thus, the western end of the central Garlock would propagate with progressively more southwesterly strikes relative to an inferred original $\sim 075^\circ$ strike of the east-central and eastern sections of the fault (Figures 2b–2d). Eventually, the southwestward propagating Garlock intersected the SAF (Figure 2d), likely along the preexisting normal fault (Figure 2c), establishing the mechanically efficient conjugate fault pair that prevails today.

The timing of this event remains poorly constrained, but the geometry of the SAF and the slip rate of the western segment of the Garlock fault can be used to infer a minimum-possible age of Garlock-SAF intersection. If the SAF through the future region of the Big Bend initially had a relatively linear NW local strike (Matti & Morton, 1993), then the portion of the SAF north of its intersection with the Garlock fault has been warped 25 ± 5 km to the southwest by sinistral motion along the Garlock fault (Bohannon & Howell, 1982; Davis & Burchfiel, 1973; Garfunkel, 1974; Stuart, 1991; Figures 2d and 2e). Assuming $\sim 25 \pm 5$ km of bending of the SAF by southwestward motion of the Sierra Nevada-Great Valley block with the current ~ 7.5 mm/year slip rate (McGill et al., 2009) suggests that Garlock fault-induced warping of the SAF could have begun as recently as circa 3 Ma. But if the early phases of slip along the newly established, mechanically immature western Garlock occurred at slower rates than the current 7.5 mm/year, then the ~ 25 km of SAF bending could

have taken much longer than 3 Myr, and the Garlock could have reached the SAF at an earlier date. Indeed, earlier contractional deformation manifest in early Pliocene (4–6 Ma) exhumation documented by Apatite (U-Th)/He thermochronology within the Big Bend region (Niemi et al., 2013) is consistent with an earlier initiation of the Big Bend. This onset of accelerated exhumation rates in the Big Bend area circa 4–6 Ma (Niemi et al., 2013) suggests that the current efficient conjugate pairing of the SAF and the Garlock fault had been established prior to the onset of the earliest well-developed NNW-trending faults in the currently active ECSZ circa 3–4 Ma, when the Death Valley, Panamint Valley, and Owens Valley fault systems all began to accommodate rapid dextral shear (Burchfiel et al., 1987; Lee et al., 2009; Monastero et al., 2002; Norton, 2011) and dextral slip began in the southern ECSZ on the Blackwater fault (Andrew et al., 2014; Andrew & Walker, 2017; Oskin & Iriondo, 2004).

Whether the Garlock fault reached the SAF at 3 Ma or somewhat earlier, the full extent of the Garlock fault developed with minimal contribution due to dextral slip within the northern and southern ECSZ fault rotation from ECSZ dextral shear (Figure 2d). Palinspastic reconstructions suggest that there may have been distributed dextral shear in the southern ECSZ as early as 8–12 Ma (McQuarrie & Wernicke, 2005) which could have resulted in some clockwise rotation of the central and eastern Garlock fault prior to the initiation of well-developed, high-slip rate faults in the ECSZ. We note that any such distributed dextral shear prior to the circa 3–4 Ma onset of the currently active ECSZ dextral fault system would render the rotation-induced sinistral slip rate estimates for the central and eastern Garlock that we calculate in the following section as maximum values—the true, full 11 Ma rotation-induced sinistral slip rates must be slower if there was any distributed dextral shear across the Garlock prior to 3–4 Ma.

5. Controls on Current Garlock Fault Slip Rates

Geologic slip rates determined along the Garlock fault provide key kinematic observations that help to constrain a comprehensive mechanical model for the ongoing activity of the Garlock fault. We use geologic slip rates that are at least of mid-Holocene to latest Pleistocene age as constraints (supporting information Table S1). This age requirement intentionally excludes some young (<4 ka), fast rates observed on the central segment (Dolan et al., 2016; Rittase et al., 2014) because these rates encompass a four-event earthquake cluster at 0.5–2 ka during which the fault was slipping far faster than its long-term average rate (Dawson et al., 2003; Dolan et al., 2007, 2016; Ganey et al., 2012). Integration of the long-term, mid-Holocene to latest Pleistocene fault slip rates with our model of fault evolution allows us to assess the relative along-strike contributions of each of the three kinematic models that have been proposed to drive the Garlock fault.

5.1. Contribution From Rotation of the Garlock Fault Due to ECSZ Dextral Shear

We calculate the contribution to sinistral slip rate along the Garlock fault due to oroclinal bending of the fault by NNW oriented ECSZ dextral shear by quantifying the difference in length between the initial and present-day traces (Figure 3). The present-day Garlock fault must have lengthened from its initial, undeflected state as dextral shear in the ECSZ north and south of the Garlock fault has rotated the fault clockwise and, in the process, extended the length of the Garlock fault. Purple dots in Figure 3a mark deviations from the preferred initial proposed fault strike of 075°, which correspond to increases in dextral shear rate across the Garlock fault, and are thus pivot points, or fulcrums, that mark changes in the rate of ECSZ dextral slip-induced clockwise rotation of the Garlock fault. The initial geometry of the Garlock fault is shown as a gray, dashed line, whereas the current, rotated geometry of the Garlock fault is shown by the solid purple line (Figure 3a).

As discussed in the previous section, the preferred initial ENE geometry of the central and eastern Garlock is approximately perpendicular to the NNW orientation of the main northern ECSZ faults. Hence, as shown in Figure 3b, we can envisage a triangle with a right angle between the trend of the ECSZ and the initial Garlock fault, and with an angle θ between the initial and present-day strikes of the Garlock fault. The leg of the triangle adjacent to θ represents the initial Garlock fault, and the hypotenuse represents the present-day Garlock fault (Figure 3b). The opposite side of this triangle represents the amount of dextral ECSZ slip that has occurred since initiation of dextral shear in the ECSZ to produce the Garlock fault rotation. As the ECSZ accommodates dextral shear over time, the leg of the triangle opposite θ in Figure 3b must grow. As that leg grows, the hypotenuse must also lengthen, showing that the Garlock fault must lengthen to

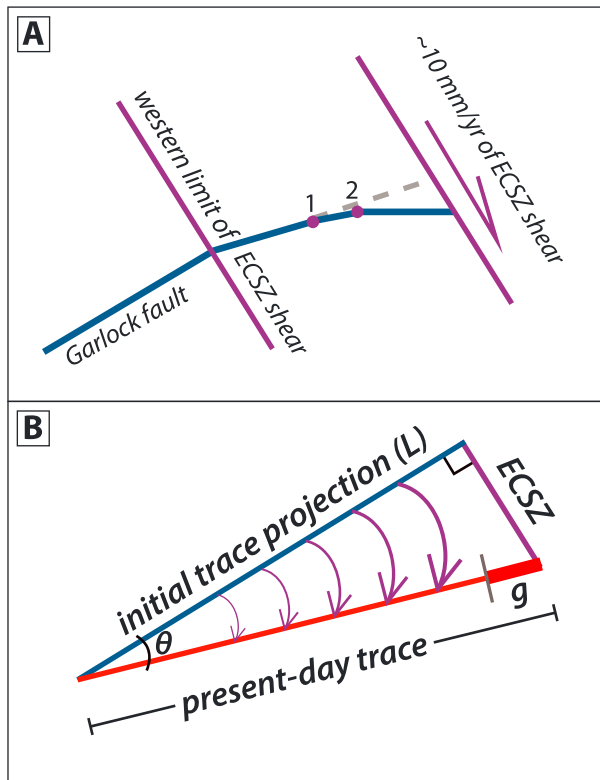


Figure 3. Schematic diagrams detailing rotational contribution calculations. (a) The Garlock fault (blue line segments) is progressively deformed by dextral shear along NNW trending ECSZ faults at ~ 10 mm/year. We assume that the Garlock fault bends at pivot points (fulcrums) associated with intersections between the Garlock and individual ECSZ faults; these fulcrums are located east of the Blackwater fault (1) and the Panamint Valley fault zone near Pilot Knob Valley (2), and represent the changes in fault strike along the central and eastern segments of the Garlock fault. The rate of dextral shear increases eastward at each successive intersection of the Garlock fault with an ECSZ fault, commensurately increasing the amount of clockwise rotation of the Garlock eastward. Purple lines denote western and eastern boundaries of NNW directed dextral ECSZ. No dextral shear is assumed to occur outside of these boundaries. Purple dots show key positions along the Garlock fault at which major changes in cumulative rotation are observed. Purple dot 1 shows the location of a slight clockwise change in strike of central segment of Garlock fault, and purple dot 2 shows the more pronounced change in Garlock fault strike at the central-eastern segment boundary. (b) Schematic illustration of how we estimate the component of sinistral Garlock fault slip related to ECSZ-induced clockwise rotation of the Garlock. The inferred original strike of the Garlock fault is shown by the blue line. The purple line represents total ECSZ dextral shear across the entire system. This dextral shear, which decreases westward to zero at the western boundary of the ECSZ, induces clockwise rotation of the Garlock fault (shown schematically by purple arrows). As the Garlock fault rotates, it will lengthen. The rotated, current Garlock fault trace (thin red line) is longer than the initial trace projection (blue line) by a finite amount g (thick red line), which is the difference between the hypotenuse (red) and adjacent (blue) legs in this triangle. As discussed in the text, we use g to estimate the component of Garlock fault slip that is driven by ECSZ dextral shear-induced clockwise rotation and lengthening of the Garlock fault. ECSZ = eastern California shear zone.

accommodate continued dextral shear in the ECSZ. Under these assumptions, the present-day Garlock must be longer than the initial Garlock. We use the following equation to calculate how much the present-day Garlock fault must have grown relative to the initial fault:

$$g = L / \cos\theta - L$$

where g is the amount of growth, or lengthening, of the Garlock fault due to ECSZ dextral shear-induced clockwise rotation of the Garlock, L is the length of the initial trace of the Garlock (adjacent leg of the triangle in Figure 3b—the initial length of the Garlock fault), and θ is the angle between the initial and present-day traces of the Garlock fault.

For this exercise, we assume spatially uniform strikes of the present-day east-central and eastern segments of the Garlock of $\sim 078^\circ$ and $\sim 092^\circ$, respectively. Because total dextral shear rate increases progressively eastward at each intersection with major ECSZ faults, the amount of total southward deflection of the Garlock is greatest at the eastern end. The change in length of the Garlock fault between the inferred initial strike and the longer, present-day fault represents the *growth* of the Garlock fault required for lengthening the fault; this lengthening of the Garlock fault denotes the resulting amount of sinistral fault slip on the Garlock fault as it was oroclinally rotated by ECSZ dextral shear (Figure 3b). The resulting contributions to Garlock fault slip due to rotation will increase at each of the fulcrum points at each distinct change in present-day strike. Specifically, these pivot points (denoted by purple dots in Figure 3a) are located at the western end of the ECSZ-induced rotation field along the western end of the central segment of the Garlock fault at the western edge of significant dextral ECSZ shear and at the central to eastern Garlock fault segment boundary for the eastern segment.

We use the circa 3 Ma initiation of significant ECSZ dextral shear (Andrew & Walker, 2017; Andrew et al., 2014; Burchfiel et al., 1987; Lee et al., 2009; Monastero et al., 1997; Norton, 2011; Oskin & Iriondo, 2004) to calculate the rotation-induced component of sinistral Garlock fault slip rate. As noted above, the following estimates do not consider any pre-3 Ma clockwise rotation of the Garlock that may have occurred in response to an earlier phase of distributed dextral shear in the Mojave prior to establishment of the well-developed, currently active ECSZ faults by circa 3 Ma. Thus, the rates we calculate will be maxima, as we are assuming that all of the rotation has occurred within the minimum 3-My period since the establishment of discrete NNW faulting within the ECSZ.

The resulting rotation-induced sinistral Garlock rate using a preferred initial strike of 075° and an initial fault length of 25 km (the length of the eastern part of the Garlock fault central segment that is oriented at strikes greater than 075°) is extremely slow on the east-central Garlock fault, with a maximum rate of 0.01 mm/year due to the small amount of rotation ($\sim 3^\circ$; Figure 4). However, the 50-km-long eastern segment has rotated more ($\sim 17^\circ$ relative to an initial 075° strike), yielding a larger rotational contribution to sinistral Garlock slip that reaches

a maximum of ~ 0.8 mm/year at the eastern end of the fault. It is noteworthy that this rotation-induced sinistral rate is similar to the preferred ~ 1 mm/year slip rate documented for the eastern Garlock fault by Crane (2014). Alternatively, for an initial fault strike of 060° , the maximum sinistral slip rate of the east-central

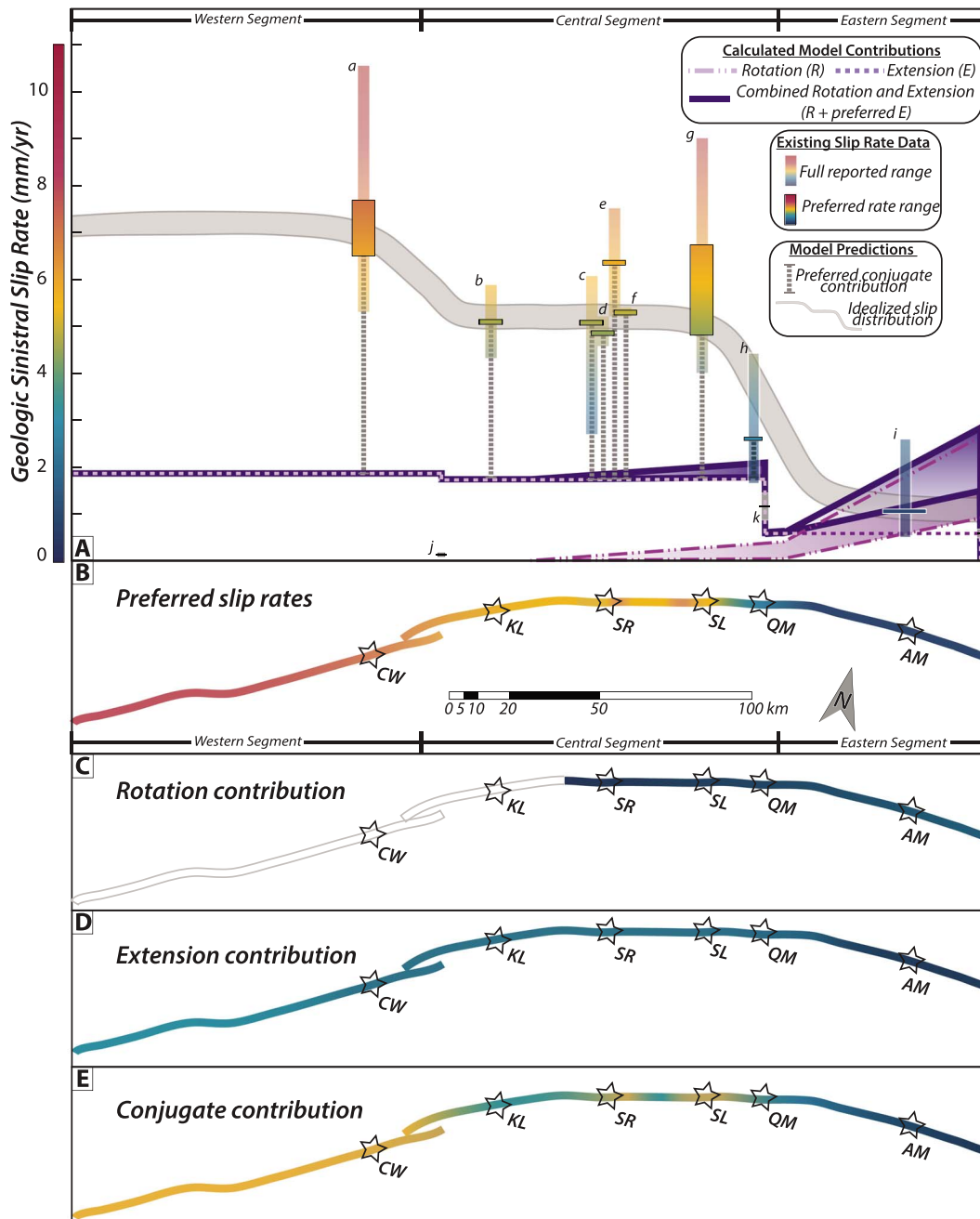


Figure 4. Garlock fault loading contributions constrained by existing slip rate data. (a) Purple lines plot the relative contributions to Garlock fault loading from ECSZ rotation (dash-dotted line), BR extension (dashed line), and combined (solid line) contribution from rotation and extension (using the mean value of Garlock-parallel extension rates from ranges reported in text). Rotation-induced sinistral rates include end-member cases of 060° and 075° initial orientation of the Garlock fault, and rotation rate ranges and consequent extension and rotation combined contributions are represented with purple shaded polygons. Available Garlock geologic slip rates (a–l; see supporting information Table S1). Locations of slip rate sites are shown in Figure 1 and on the lower panel of this figure. Slip rates are plotted with reported full ranges (transparent, narrow bars) and preferred ranges (opaque, wide bars) and are colored according to color bar on y axis. Vertical gray dashed bars represent slip rate deficit between combined rotation + extension contribution and the preferred slip rate at each site, showing the assumed contribution to slip rate from conjugate shear. Broad gray curve shows idealized slip rate distribution along strike. (b) Garlock fault map colored by preferred geologic slip rate; same slip rate color scale as in upper panel. (c) ECSZ-driven rotation contribution BR, (d) extensional contribution, and (e) conjugate contribution to the preferred geologic slip. Stars representing slip rates are CW = Clark Wash; KL = Koehn Lake; SR = Summit Range; SL = Searles Lake; QM = Quail Mountains; AM = Avawatz Mountains. ECSZ = eastern California shear zone; BR = Basin and Range.

Garlock increases to 0.4 mm/year, and to 2.7 mm/year at the eastern end of the Garlock, at or faster than the extreme high end of the observed eastern Garlock slip rate of $1 \pm_{-0.5}^{+1.5}$ mm/year (Crane, 2014).

5.2. Contribution From BR Extension

Because the rotation model does not generate sufficient sinistral slip to explain the behavior of the entire Garlock, especially for the faster-slipping central and western segments, we explore the slip contribution due to BR extension north of the fault. This component increases westward in an additive sense as each successive BR fault is crossed, from a minimum at the southern end of Death Valley to a maximum at the Sierra Nevada Frontal fault (Davis & Burchfiel, 1973; McGill et al., 2009).

We used extension rates from BR normal and ECSZ oblique-dextral faults north of the Garlock, specifically the Sierra Nevada Frontal, Panamint Valley, and Death Valley dextral-normal faults, to calculate Garlock-parallel extension rates. We projected these extension rates (supporting information Table S1) onto the local strike of the eastern and central segments of the Garlock fault. The resulting Garlock-parallel sinistral slip rates are 0.5–0.7 mm/year from the Death Valley fault, 0.9–1.5 mm/year from the Panamint Valley fault, and 0.1–0.2 mm/year from the Sierra Nevada Frontal fault (Frankel et al., 2015; Hoffman, 2009; Le et al., 2007). The maximum cumulative BR extension contribution to Garlock fault slip is therefore 1.5–2.4 mm/year, at and extending to the west of the Sierra Nevada Frontal fault (Figure 4).

5.3. Contribution From Conjugate Relationship to SAF

The combined BR extensional and ECSZ rotational components of Garlock slip in our model match the slow ($1 \pm_{-0.5}^{+1.5}$ mm/year) slip rate documented by Crane (2014) for the eastern Garlock fault (Figure 4), especially for an initial inferred fault orientation of 075° , suggesting that the current slip rate of the eastern segment is adequately explained by these mechanisms. However, these summed slip rate components are insufficient to explain the faster rates on the central and western segments. This slip rate discrepancy indicates that conjugate slip must contribute the difference between the combined extension-rotation contributions and the measured slip rates on the western and central segments (Figure 3). For example, the preferred slip rate of the western segment is ≤ 7.5 mm/year (McGill et al., 2009; S. F. McGill, personal communication, 2018). Because the western Garlock is not deformed by dextral shear in the ECSZ (i.e., the rotational contribution to slip is 0 mm/year), BR extension contributes only ~ 1.5 – 2.5 mm/year of sinistral slip to the western Garlock, indicating that conjugate motion accounts for the remaining ~ 5 – 6 mm/year of the preferred ~ 7.5 mm/year western Garlock fault slip rate measured by McGill et al. (2009). Similarly, the slip rate of the central Garlock, which is well constrained from a number of sites at ~ 5 – 6 mm/year (Clark & Lajoie, 1974; Crane, 2014; Dolan et al., 2015; Ganey et al., 2012; McGill & Sieh, 1993), exceeds the combined contributions of sinistral slip due to BR extension and ECSZ shear of ~ 1.5 – 2.5 mm/year, indicating that conjugate slip contributes the remaining ~ 3 – 4 mm/year to the central Garlock slip rate. Because the current slip rate of the eastern segment of the Garlock fault can be explained solely by contributions from the ECSZ rotational and BR extensional mechanisms, we suggest that little to none of the current slip on the eastern segment is due to conjugate behavior.

6. Implications for Fault Interactions, Earthquake Recurrence, and Plate Boundary Evolution in Southern California

Because it is driven by a combination of SAF conjugate shear, BR extension, and ECSZ-induced rotation, the Garlock fault can store elastic strain energy under multiple loading regimes depending on which of the three driving mechanisms were most active at any given time. Understanding these relationships will thus provide insight into spatiotemporal patterns of earthquake occurrence and fault slip on the Garlock and neighboring faults. Moreover, these complex kinematic relationships suggest that the Garlock fault acts as a mechanical bridge connecting slip on the Mojave SAF (mSAF) and southern SAF (sSAF) with slip on faults in the BR and ECSZ north of the Garlock (NECSZ) (Figure 5). The NECSZ-GF-mSAF-sSAF fault network creates a closed kinematic loop that acts as an efficient, mechanically complementary alternative to N-S dextral shear in the ECSZ-Walker Lane-sSAF system. As a result, strain transfer via the Garlock fault enables the mSAF to accommodate dextral shear that would otherwise be accommodated on the ECSZ south of the Garlock (SECSZ).

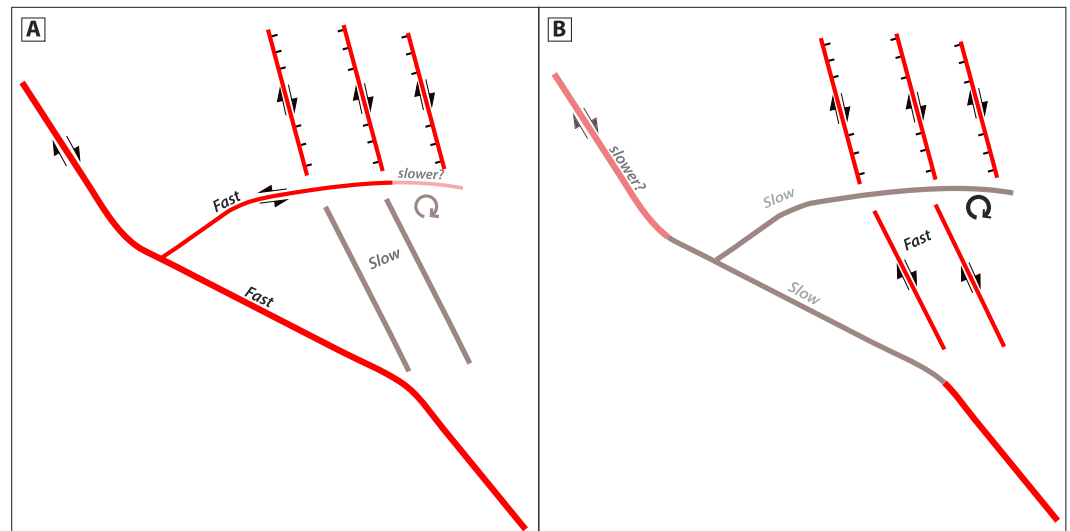


Figure 5. Schematic map showing the two proposed strain accumulation and accommodation systems in Southern California, highlighting alternation between fault activities between faster (black) and slower (gray) rates in each subsystem relative to long-term geologic strain accommodation rate. Modified from Dolan et al. (2007). (a) Fast, high strain accommodation Garlock fault. (b) Slow, low strain accommodation Garlock fault.

The occurrence of large historic earthquakes (1872 $M_w \sim 7.6$ Owens Valley, 1992 $M_w = 7.3$ Landers, and 1999 $M_w = 7.1$ Hector Mine) and several recent prehistoric surface ruptures on the Panamint Valley and Death Valley faults, as well as on several faults in the SECSZ (Frankel et al., 2008; Ganev et al., 2012; McAuliffe et al., 2013; Rockwell et al., 2000), attest to recent rapid strain release on the throughgoing ECSZ subsystem. Conversely, the Garlock has generated only one surface rupture in the past 1,000–1,200 years, and none in the past circa 500 years (Dawson et al., 2003; Madugo et al., 2012), despite a relatively rapid average long-term slip rate. Moreover, most models of geodetic data suggest present-day elastic strain accumulation rates that are much slower than the average Garlock fault slip rate (e.g., Evans et al., 2016; Loveless & Meade, 2011; McClusky et al., 2001; Meade & Hager, 2005; Peltzer et al., 2001). These data suggest that the subsystem including the Garlock fault is currently storing and releasing strain energy at much slower than average rates while the ECSZ subsystem is releasing energy at faster than average rates. The recognition of millennia-long strain supercycles along the Garlock and related faults suggests that the apparent alternation between these two subsystems may persist over longer time-scales (Dolan et al., 2016).

Further complicating this behavior is the fact that the SAF stores and releases strain much faster than any other fault in the plate boundary system. Thus, because the western and central segments of the Garlock fault are loaded primarily by conjugate shear-related strain accumulation, the Garlock will accumulate and accommodate strain faster when the SAF is slipping faster. Conversely, the eastern Garlock is loaded primarily by ECSZ dextral shear-induced rotation and will therefore accumulate and accommodate strain primarily in response to the behavior of the ECSZ. The central segment of the Garlock, which is loaded by both conjugate shear and BR extension, might be expected to experience very complicated patterns of strain accumulation and release controlled by the relative rates of the two driving mechanisms.

In general, available paleoearthquake and incremental fault slip rate data are too incomplete to fully evaluate our proposed multimechanism Garlock loading model. However, where the data are of sufficient density and precision, as along the mSAF and central Garlock, they support our model results. For example, as noted by Dolan et al. (2016), the two most-recent central Garlock earthquakes observed at El Paso Peaks (circa 0.5 and 1.0 ka; Dawson, 2003), correlate closely in time with an anomalously large-magnitude mSAF earthquake and a period of highly accelerated mSAF slip rate observed at the Wrightwood paleoseismic site (Weldon et al., 2004), consistent with the predominant, conjugate-loading mechanism we suggest for the western and central Garlock fault. Unfortunately, detailed incremental slip rate data are not available for mSAF prior to circa 1.5 ka, and thus, we cannot evaluate whether the two earlier earthquakes in the 0.5–2.0 ka central Garlock

cluster (circa 1.5–1.75 ka and 1.75–2.0 ka; Dawson, 2003) were related to either anomalously rapid slip and/or particularly large SAF earthquakes.

The location of the 1992 M_w 7.3 Landers earthquake led to the suggestion that this earthquake was a harbinger of an eventual eastward jump in the Pac-NAM plate boundary from the SAF system to east of the Sierra Nevada along the ECSZ-Walker Lane (Du & Aydin, 1996; Faulds et al., 2005; Nur et al., 1993; Spotila & Anderson, 2004; Thatcher et al., 2016; Yang & Hauksson, 2013). This inference is based on the assumption that events such as Landers, which connected parts of six different ECSZ faults together to form an overall more linear north-trending rupture, will eventually create a throughgoing N-S zone of dextral shear that could more efficiently accommodate Pac-NAM plate motion by bypassing the mechanical complexities of the SAF system in Southern California (e.g., the Big Bend and San Gorgonio knot) (Nur et al., 1993).

Although this model is attractive in its simplicity, and earthquakes such as Landers suggest that such a plate boundary switch may eventually occur, a key observation is that no ECSZ faults extend across the Garlock fault (e.g., Andrew & Walker, 2017; Andrew et al., 2014; Davis & Burchfiel, 1973; Dokka & Travis, 1990b; Garfunkel, 1974; Glazner et al., 2002; Oskin & Iriondo, 2004), despite at least 3 million years of N-S dextral shear and current geodetic data suggesting that dextral shear extends across the Garlock fault (Gan et al., 2000; Lee et al., 2009; McClusky et al., 2001; McGill et al., 2009; Monastero et al., 2002; Norton, 2011; Peltzer et al., 2001). Given these observations, the question arises, why has such a throughgoing fault system not yet developed?

We propose that the mechanical efficiency of the Garlock fault, in providing an alternative pathway for dextral ECSZ shear, reduces the need for this postulated eastward shift. Continued activity along the Garlock thus maintains the long-term stability of the current plate boundary configuration, including the mechanical inefficiency of the Big Bend of the San Andreas. Loading of the Garlock fault by both conjugate SAF slip and BR extension will continue to be accommodated effectively by Garlock fault slip, at least whenever the NECSZ-Garlock-mSAF-sSAF subsystem is active. However, ongoing sinistral Garlock slip will also continue to amplify the curvature of the Big Bend, making this part of the SAF less and less mechanically efficient in accommodating Pac-NAM plate boundary dextral shear. If, eventually, increasing misalignment of the SAF at the Big Bend caused by continued Garlock fault slip renders the SAF too inefficient to effectively accommodate Pac-NAM motion, and if fault growth and linkage similar to those that occurred in the Landers earthquake continue, a mechanically efficient, throughgoing N-S zone of dextral shear east of the Sierra Nevada may yet become established. Until then, however, the Garlock fault will continue to provide an alternative stair-step means of north-south transfer of Pac-NAM shear via conjugate fault pairs for the foreseeable future.

Acknowledgments

We thank Charles Sammis, Joe Andrew, and Robert Zinke for helpful discussions; Sally McGill, Nadine McQuarrie, and Doug Walker for thoughtful and constructive reviews; and Greg Davis for class term project guidance for A. E. H. Data are available in supporting information Table S1 and Figure 4; readers may contact A. E. H. for further data inquiries.

References

- Andrew, J. E., & Walker, J. D. (2017). Path and amount of dextral fault slip in the eastern California shear zone across the central Mojave Desert. *Geological Society of America Bulletin*, 129(7–8), 855–868. <https://doi.org/10.1130/B31527.1>
- Andrew, J. E., Walker, J. D., & Monastero, F. C. (2014). Evolution of the central Garlock fault zone, California: A major sinistral fault embedded in a dextral plate margin. *Bulletin Geological Society of America*, 127(1–2), 227–249. <https://doi.org/10.1130/B31027.1>
- Armijo, R., Flerit, F., King, G., & Meyer, B. (2004). Linear elastic fracture mechanics explains the past and present evolution of the Aegean. *Earth and Planetary Science Letters*, 217(1–2), 85–95. [https://doi.org/10.1016/S0012-821X\(03\)00590-9](https://doi.org/10.1016/S0012-821X(03)00590-9)
- Atwater, T. (1970). Implications of plate tectonics for the Cenozoic tectonic evolution of western North America. *Geological Society of America Bulletin*, 81(12), 3513. [https://doi.org/10.1130/0016-7606\(1970\)81\[3513:IOPTFT\]2.0.CO;2](https://doi.org/10.1130/0016-7606(1970)81[3513:IOPTFT]2.0.CO;2)
- Blythe, A. E., & Longinotti, N. (2013). Exhumation of the southern sierra Nevada–Eastern Tehachapi Mountains constrained by low-temperature thermochronology: Implications for the initiation of the Garlock fault. *Lithosphere*, 5(3), 321–327. <https://doi.org/10.1130/L252.1>
- Bohannon, R. G., & Howell, D. G. (1982). Kinematic evolution of the junction of the San Andreas, Garlock, and Big Pine faults, California. *Geology*, 10, 358–363. [https://doi.org/10.1130/0091-7613\(1982\)10<358](https://doi.org/10.1130/0091-7613(1982)10<358)
- Bowman, D., King, G., & Tapponnier, P. (2003). Slip partitioning by elastoplastic propagation of oblique slip at depth. *Science*, 300(5622), 1121–1123. <https://doi.org/10.1126/science.1082180>
- Burbank, D. W., & Whistler, D. P. (1987). Temporally constrained tectonic rotations derived from magnetostratigraphic data: Implications for the initiation of the Garlock fault, California. *Geology*, 15(12), 1172–1175. [https://doi.org/10.1130/0091-7613\(1987\)15<1172:TCTTRDF>2.0.CO;2](https://doi.org/10.1130/0091-7613(1987)15<1172:TCTTRDF>2.0.CO;2)
- Burchfiel, B. C., Hodges, K. V., & Royden, L. H. (1987). Geology of Panamint Valley - Saline Valley pull apart system, California: Palinspastic evidence for low-angle geometry of a Neogene range-bounding fault. *Journal of Geophysical Research*, 92(B10), 10,422–10,426. <https://doi.org/10.1029/JB092iB10p10422>
- Burke, D. B., & Clark, M. M. (1978). Late Quaternary activity along Garlock fault at Koehn Lake, Fremont Valley, California. In *Transactions-American Geophysical Union*, (p. 1126). Washington, DC: American Geophysical Union.
- Chapman, A., Saleeby, J. B., Wood, D. J., Piasecki, A., Kidder, S., Ducea, M. N., & Farley, K. A. (2012). Late Cretaceous gravitational collapse of the southern Sierra Nevada batholith, California. *Geosphere*, 8(2), 314. <https://doi.org/10.1130/GES00740.1>
- Clark, M. M. (1973). Map showing recently active breaks along the Garlock fault and associate faults, California, scale 1:24,000, *U.S. Geol. Surv., Map 1-741*, 3 sheets.

- Clark, M. M., & Lajoie, K. R. (1974). Holocene behavior of the Garlock fault, in *Geological Society of America Abstracts with Programs (Cordilleran Section)*, volume 6.
- Crane, T. M. (2014). *Qualitative comparison of offset surfaces between the central and eastern Garlock fault*. San Bernardino: California State University.
- Davis, G. A., & Burchfiel, B. C. (1973). Garlock fault: An intracontinental transform structure, Southern California. *Geological Society of America Bulletin*, 84(4), 1407–1422. [https://doi.org/10.1130/0016-7606\(1973\)84<1407:GFAITS>2.0.CO;2](https://doi.org/10.1130/0016-7606(1973)84<1407:GFAITS>2.0.CO;2)
- Dawson, T. E. (2003). Irregular recurrence of paleoearthquakes along the central Garlock fault near El Paso Peaks, California. *Journal of Geophysical Research*, 108(B7), 2356. <https://doi.org/10.1029/2001JB001744>
- Dawson, T. E., McGill, S. F., & Rockwell, T. K. (2003). Irregular recurrence of paleoearthquakes along the central Garlock fault near El Paso Peaks, California. *Journal of Geophysical Research*, 108(B7), 2356. <https://doi.org/10.1029/2001JB001744>
- DeMets, C., Gordon, R. G., & Argus, D. F. (2010). Geologically current plate motions. *Geophysical Journal International*, 181(1), 1–80. <https://doi.org/10.1111/j.1365-246X.2009.04491.x>
- Dokka, R. K., & Travis, C. J. (1990a). Late Cenozoic strike-slip faulting in the Mojave Desert, California. *Tectonics*, 9(2), 311–340. <https://doi.org/10.1029/TC009i002p00311>
- Dokka, R. K., & Travis, C. J. (1990b). Role of the eastern California shear zone in accommodating Pacific North American plate motion. *Geophysical Research Letters*, 17(9), 1323–1326. <https://doi.org/10.1029/GL017i009p01323>
- Dolan, J. F., Bowman, D. D., & Sammis, C. G. (2007). Long-range and long-term fault interactions in Southern California. *Geology*, 35(9), 855–858. <https://doi.org/10.1130/G23789A.1>
- Dolan, J. F., McAuliffe, L. J., Rhodes, E. J., McGill, S. F., & Zinke, R. (2016). Extreme multi-millennial slip rate variations on the Garlock fault, California: Strain super-cycles, potentially time-variable fault strength, and implications for system-level earthquake occurrence. *Earth and Planetary Science Letters*, 446, 123–136. <https://doi.org/10.1016/j.epsl.2016.04.011>
- Dolan, J. F., McGill, S. F., & Rhodes, E. J. (2015). A new mid-Holocene slip rate for the central Garlock fault: Implications for the constancy of fault slip rates and system-level fault behavior, in *Southern California Earthquake Center Annual Meeting Proceedings Volume XXV*, p. 144.
- Du, Y., & Aydin, A. (1996). Is the San Andreas big bend responsible for the Landers earthquake and the eastern California shear zone? *Geology*, 24(3), 219–222. [https://doi.org/10.1130/0091-7613\(1996\)024<0219:ITSABB>2.3.CO;2](https://doi.org/10.1130/0091-7613(1996)024<0219:ITSABB>2.3.CO;2)
- Eaton, J. E. (1932). Decline of Great Basin, southwestern United States. *American Association of Petroleum Geologists Bulletin*, 16(1), 1–49.
- Evans, E. L., Thatcher, W. R., Pollitz, F. F., & Murray, J. R. (2016). Persistent slip rate discrepancies in the eastern California (USA) shear zone. *Geology*, 44(9), 691–694. <https://doi.org/10.1130/G37967.1>
- Faulds, J. E., Henry, C. D., & Hinz, N. H. (2005). Kinematics of the northern Walker Lane: An incipient transform fault along the Pacific – North American plate boundary. *Geology*, 33(6), 505–508. <https://doi.org/10.1130/G21274.1>
- Flerit, F., Armijo, R., King, G., & Meyer, B. (2004). The mechanical interaction between the propagating North Anatolian fault and the back-arc extension in the Aegean. *Earth and Planetary Science Letters*, 224(3–4), 347–362. <https://doi.org/10.1016/j.epsl.2004.05.028>
- Frankel, K. L., Glazner, A. F., Kirby, E., Monastero, F. C., Strane, M. D., Oskin, M. E., et al. (2008). Active tectonics of the eastern California shear zone. *Geological Society of America, Field Guide*, (9), 27–38. <https://doi.org/10.1130/2008.fl>
- Frankel, K. L., Owen, L. A., Dolan, J. F., Knott, J. R., Lifton, Z. M., Finkel, R. C., & Wasklewicz, T. (2015). Timing and rates of Holocene normal faulting along the Black Mountains fault zone, Death Valley, USA. *Lithosphere*, 8(1), 3–22. <https://doi.org/10.1130/L464.1>
- Gan, W., Svarc, J. L., Savage, J. C., & Prescott, W. H. (2000). Strain accumulation across the eastern California shear zone at latitude 36°30'N. *Journal of Geophysical Research*, 105(B7), 16,299–16,236.
- Ganev, P. N., Dolan, J. F., McGill, S. F., & Frankel, K. L. (2012). Constancy of geologic slip rate along the central Garlock fault: Implications for strain accumulation and release in southern California. *Geophysical Journal International*, 190(2), 745–760. <https://doi.org/10.1111/j.1365-246X.2012.05494.x>
- Garfunkel, Z. (1974). Model for the Late Cenozoic tectonic history of the Mojave Desert, California, and for its relation to adjacent regions. *Bulletin Geological Society of America*, 85(December), 1931. [https://doi.org/10.1130/0016-7606\(1974\)85<1931](https://doi.org/10.1130/0016-7606(1974)85<1931)
- Glazner, A. F., Walker, J. D., Bartley, J. M., & Fletcher, J. M. (2002). Cenozoic evolution of the Mojave block of Southern California. In A. F. Glazner, J. D. Walker, & J. M. Bartley (Eds.), *Geologic evolution of the Mojave Desert and southwestern Basin and Range Geological Society of America Memoir 195*, (pp. 19–42). Boulder, CO: Geological Society of America.
- Guest, B., Pavlis, T. L., Golding, H., & Serpa, L. (2003). Chasing the Garlock: A study of tectonic response to vertical axis rotation. *Geology*, 31(6), 553–556. [https://doi.org/10.1130/0091-7613\(2003\)031<0553](https://doi.org/10.1130/0091-7613(2003)031<0553)
- Hatem, A. E., & Dolan, J. F. (2015). Garlock fault: What is your deal, in *Southern California Earthquake Center Annual Meeting, poster 233*, Palm Springs.
- Hill, M. L., & Dibblee, T. W. J. (1953). San Andreas, Garlock and Big Pine faults, California. *Geological Society of America Bulletin*, 64(4), 443–468. [https://doi.org/10.1130/0016-7606\(1953\)64\[443:SAGABP\]2.0.CO;2](https://doi.org/10.1130/0016-7606(1953)64[443:SAGABP]2.0.CO;2)
- Hoffman, W. R. (2009). *Late Pleistocene slip rates along the Panamint Valley fault zone, eastern California*. State College, PA: Pennsylvania State University.
- Humphreys, E. D., & Weldon, R. J. (1994). Deformation across the western United States: A local estimate of Pacific-North America transform deformation. *Journal of Geophysical Research*, 99(B10), 19,975–20,010.
- Jahns, R., Troxel, B. W., & Wright, L. A. (1971). Some structural implication of a late Precambrian–Cambrian section in the Avawatz Mountains, California. *Geological Society of America Abstracts with Programs (Cordilleran Section)*, 3(2), 140.
- Jennings, C. W. (1994). Fault activity map of California and adjacent areas. *Department of Conservation, Division of Mines and Geology*.
- King, G. C., Friedrich, A., Armijo, R., Gaudemer, Y., & Bowman, D. (2004). Speculations on the evolution of the east California shear zone and associated structures by fault propagation: Comparison with the mechanics of Anatolia and the Aegean, in *American Geophysical Union, Fall Meeting 2004, abstract #T31A-1258*.
- Le, K., Lee, J., Owen, L. A., & Finkel, R. (2007). Late Quaternary slip rates along the Sierra Nevada frontal fault zone, California: Slip partitioning across the western margin of the eastern California shear zone–Basin and Range province. *Bulletin Geological Society of America*, 119(1–2), 240–256. <https://doi.org/10.1130/B25960.1>
- Lee, J., Stockli, D. F., Owen, L. A., Finkel, R. C., & Kisilitsyn, R. (2009). Exhumation of the Inyo Mountains, California: Implications for the timing of extension along the western boundary of the Basin and Range Province and distribution of dextral fault slip rates across the eastern California shear zone. *Tectonics*, 28, TC1001. <https://doi.org/10.1029/2008TC002295>
- Loveless, J. P., & Meade, B. J. (2011). Stress modulation on the San Andreas fault by interseismic fault: System interactions. *Geology*, 39(11), 1035–1038. <https://doi.org/10.1130/G32215.1>
- Luyendyk, B. P. (1991). A model for Neogene crustal rotations, transtension, and transpression in southern California. *Geological Society of America Bulletin*, 103(11), 1528–1536. [https://doi.org/10.1130/0016-7606\(1991\)103<1528:AMFNCR>2.3.CO;2](https://doi.org/10.1130/0016-7606(1991)103<1528:AMFNCR>2.3.CO;2)

- Luyendyk, B. P., Kamerling, M. J., & Terres, R. (1980). Geometric model for Neogene crustal rotations in southern California Geometric model for Neogene crustal rotations in Southern California. *Geological Society of America Bulletin*, 91, 211–217. [https://doi.org/10.1130/0016-7606\(1980\)91<211](https://doi.org/10.1130/0016-7606(1980)91<211)
- Madugo, C. M., Dolan, J. F., & Hartleb, R. D. (2012). New paleoearthquake ages from the western Garlock fault: Implications for regional earthquake occurrence in Southern California. *Bulletin of the Seismological Society of America*, 102(6), 2282–2299. <https://doi.org/10.1785/0120110310>
- Malin, P. E., Goodman, E. D., Henyey, T. L., Li, Y. G., Okaya, D. A., & Saleeby, J. B. (1995). Significance of seismic reflections beneath a tilted exposure of deep continental crust, Tehachapi Mountains, California. *Journal of Geophysical Research: Solid Earth*, 100(B2), 2069–2087. <https://doi.org/10.1029/94JB02127>
- Matti, J. C., & Morton, D. M. (1993). Paleogeographic evolution of the San Andreas fault in Southern California: A reconstruction based on a new cross-fault correlation. In R. E. Powell, R. J. Weldon, & J. C. Matti (Eds.), *Geological Society of American Memoirs*, (Vol. 178, pp. 107–160). Boulder, CO: GSA Memoirs.
- McAuliffe, L. J., Dolan, J. F., Kirby, E., Rollins, J. C., Haravitch, B., Alm, S., & Rittenour, T. M. (2013). Paleoseismology of the southern Panamint Valley fault: Implications for regional earthquake occurrence and seismic hazard in Southern California. *Journal of Geophysical Research: Solid Earth*, 118, 5126–5146. <https://doi.org/10.1002/jgrb.50359>
- McClusky, S. C., Bjornstad, S. C., Hager, B. H., King, R. W., Meade, B. J., Miller, M. M., et al. (2001). Present day kinematics of the eastern California shear zone from a geodetically constrained block model. *Geophysical Research Letters*, 28(17), 3369–3372. <https://doi.org/10.1029/2001GL013091>
- McGill, S., & Rockwell, T. (1998). Ages of Late Holocene earthquakes on the central Garlock fault near El Paso Peaks, California. *Journal of Geophysical Research*, 103(B4), 7265–7279. <https://doi.org/10.1029/97JB02129>
- McGill, S. F. (1992). *Paleoseismology and neotectonics of the central and eastern Garlock fault*. California: California Institute of Technology.
- McGill, S. F., & Sieh, K. (1991). Surficial offsets on the central and eastern Garlock fault associated with prehistoric earthquakes. *Journal of Geophysical Research*, 96(B13), 21,597–21,621. <https://doi.org/10.1029/91JB02030>
- McGill, S. F., & Sieh, K. (1993). Holocene slip rate of the central Garlock fault in southeastern Searles Valley, California. *Journal of Geophysical Research*, 98(B8), 14,217–14,231. <https://doi.org/10.1029/93JB00442>
- McGill, S. F., Wells, S. G., Fortner, S. K., Kuzma, H. A., & McGill, J. D. (2009). Slip rate of the western Garlock fault, at Clark Wash, near Lone Tree Canyon, Mojave Desert California. *Bulletin Geological Society of America*, 121(3–4), 536–554. <https://doi.org/10.1130/B26123.1>
- McQuarrie, N., & Wernicke, B. P. (2005). An animated tectonic reconstruction of southwestern North America since 36 Ma. *Geosphere*, 1(3), 147–172. <https://doi.org/10.1130/GES00016.1>
- Meade, B. J., & Hager, B. H. (2005). Block models of crustal motion in southern California constrained by GPS measurements. *Journal of Geophysical Research*, 110, B03403. <https://doi.org/10.1029/2004JB003209>
- Menard, H. W., & Atwater, T. (1968). Changes in direction of sea floor spreading. *Nature*, 219(5153), 463–467. <https://doi.org/10.1038/219463a0>
- Menard, H. W., & Atwater, T. (1969). Origin of fracture zone topography. *Nature*, 222(5198), 1037–1040. <https://doi.org/10.1038/2221037a0>
- Monastero, F. C., Sabin, A. E., & Walker, J. D. (1997). Evidence for post-early Miocene initiation of movement on the Garlock fault from offset of the Cudahy Camp Formation, east-central California. *Geology*, 25(3), 247–250. [https://doi.org/10.1130/0091-7613\(1997\)025<0247:EPPEMI>2.3.CO;2](https://doi.org/10.1130/0091-7613(1997)025<0247:EPPEMI>2.3.CO;2)
- Monastero, F. C., Walker, J. D., Katzenstein, A. M., & Sabin, A. E. (2002). Neogene evolution of the Indian Well Valley, east-central California. In A. F. Glazner, J. D. Walker, & J. M. Bartley (Eds.), *Geologica evolution of the Mojave Desert and southwestern Basin and Range: Geological Society of America Memoir 195*, (pp. 199–228).
- Niemi, N. A., Buscher, J. T., Spotila, J. A., House, M. A., & Kelley, S. A. (2013). Insights from low-temperature thermochronometry into transpressional deformation and crustal exhumation along the San Andreas fault in the western transverse ranges, California. *Tectonics*, 32, 1602–1622. <https://doi.org/10.1002/2013TC003377>
- Norton, I. (2011). Two-stage formation of Death Valley. *Geosphere*, 7(1), 171–182. <https://doi.org/10.1130/GES00588.1>
- Nur, A., Ron, H., & Beroza, G. C. (1993). The nature of the Landers-Mojave earthquake line. *Science*, 261(5118), 201–203.
- Oskin, M., & Iriondo, A. (2004). Large-magnitude transient strain accumulation on the Blackwater fault, eastern California shear zone. *Geology*, 32(4), 313–316. <https://doi.org/10.1130/G20223.1>
- Oskin, M., Perg, L., Shelef, E., Strane, M., Gurney, E., Singer, B., & Zhang, X. (2008). Elevated shear zone loading rate during an earthquake cluster in eastern California. *Geology*, 36(6), 507–510. <https://doi.org/10.1130/G24814A.1>
- Peltzer, G., Crampe, F., Hensley, S., & Rosen, P. (2001). Transient strain accumulation and fault interaction in the eastern California shear zone. *Geology*, 106(B10), 21,995–22,007. <https://doi.org/10.1029/2000JB000127>
- Rittase, W. M., Kirby, E., McDonald, E., Walker, J. D., Gosse, J., Spencer, J. Q. G., & Herrs, A. J. (2014). Temporal variations in Holocene slip rate along the central Garlock fault, Pilot Knob Valley, California. *Lithosphere*, 6(1), 48–58. <https://doi.org/10.1130/L286.1>
- Rockwell, T. K., Lindvall, S., Herzberg, M., Murbach, D., Dawson, T., & Berger, G. (2000). Paleoseismology of the Johnson Valley, Kickapoo, and Homestead Valley faults: Clustering of earthquakes in the eastern California shear zone. *Bulletin of the Seismological Society of America*, 90(5), 1200–1236. <https://doi.org/10.1785/0119990023>
- Roquemore, G. R., Smith, P. E., & Banks, E. W. (1982). Holocene earthquake activity of the eastern Garlock fault in Christmas Canyon, San Bernardino County, California, in *Geological Society of America Abstracts with Programs*, p. 228.
- Schermer, E. R., Luyendyk, B. P., & Cisowski, S. (1996). Late Cenozoic structures and tectonics of the northern Mojave Desert. *Tectonics*, 15(5), 905–932. <https://doi.org/10.1029/96TC00131>
- Smith, G. I. (1962). Large lateral displacement on Garlock fault, California, as measured from offset dike swarm. *American Association of Petroleum Geologists Bulletin*, 46(1), 85–104.
- Smith, G. I., & Ketner, K. B. (1970). Lateral displacement on the Garlock fault, southeastern California, suggested by offset sections of similar metasedimentary rocks, USGS.
- Snow, J. K., & Wernicke, B. P. (2000). Cenozoic tectonism in the central basin and range: Magnitude, rate, and distribution of upper crustal strain. *American Journal of Science*, 300(9), 659–719. <https://doi.org/10.2475/ajs.300.9.659>
- Spotila, J. A., & Anderson, K. B. (2004). Fault interaction at the junction of the transverse ranges and eastern California shear zone: A case study of intersecting faults. *Tectonophysics*, 379(1–4), 43–60. <https://doi.org/10.1016/j.tecto.2003.09.016>
- Stuart, W. D. (1991). Cause of the Garlock fault. *Geological Society of America*, 23(5), 198.
- Thatcher, W., Savage, J. C., & Simpson, R. W. (2016). The eastern California shear zone as the northward extension of the southern San Andreas fault. *Journal of Geophysical Research: Solid Earth*, 121, 1–14. <https://doi.org/10.1002/2016JB013070>

- Troxel, B. W., Wrigth, L. A., & Jahns, R. H. (1972). Evidence for differential displacement along the Garlock fault zone, California. *Geological Society of America Abstracts with Programs*, 4, 250.
- Weldon, R., Scharer, K., Fumal, T., & Biasi, G. (2004). Wrightwood and the earthquake cycle: What a long recurrence record tells us about how faults work. *Geological Society of America Today*, 14(9), 4–10. [https://doi.org/10.1130/1052-5173\(2004\)014<4](https://doi.org/10.1130/1052-5173(2004)014<4)
- Wernicke, B., & Snow, J. K. (1998). Cenozoic tectonism in the central basin and range: Motion of the Sierran Great Valley block. *International Geology Review*, 40(5), 403–410. <https://doi.org/10.1080/00206819809465217>
- Wood, D. J., & Saleeby, J. B. (1997). Late cretaceous-paleocene extensional collapse and disaggregation of the southernmost sierra Nevada batholith. *International Geology Review*, 39(11), 973–1009. <https://doi.org/10.1080/00206819709465314>
- Yang, W., & Hauksson, E. (2013). The tectonic crustal stress field and style of faulting along the Pacific North America plate boundary in Southern California. *Geophysical Journal International*, 194(1), 100–117. <https://doi.org/10.1093/gji/ggt113>